J Mater Sci: Mater Med (2007) 18:797–806
DOI 10.1007/s10856-006-0004-2

Calcium phosphate formation on titanium by low-voltage electrolytic treatments

Y. Tanaka · E. Kobayashi · S. Hiromoto · K. Asami · H. Imai · T. Hanawa

Received: 22 July 2005 / Accepted: 5 December 2005 / Published online: 2 December 2006

Abstract Electrochemical treatments are expected to be effective for the coating of calcium phosphate ceramics to a titanium substrate. In the present study, two types of chronoamperometry with a step potential and a cyclic wave potential at low voltage (up to 2.0 V) and low current density were performed in Hanks' solution to modify the surface characteristics of titanium. Titanium oxide film formed by self-passivation, that formed as reconstructed film during electrochemical treatments, and a calcium phosphate layer precipitated through treatments were characterised by X-ray photoelectron spectroscopy. The thickness and compositions of the surface films and layers were quantified from the XPS results. Calcium phosphate formation during immersion in Hanks' solution for 1.0 Ms was evaluated by scanning electron microscopy with energy-dispersive X-ray spectrometry. The results confirmed that the electrolytic treatments in this study were effective to accelerate calcium phosphate formation on titanium in Hanks' solution in spite of their lower voltage than conventional methods. The results also suggested that the hydroxyl group in the surface oxide film might contribute to the formation of calcium phosphate. This technique is a promising process for the treatment of thin titanium materials.

Y. Tanaka · E. Kobayashi (✉) · T. Hanawa
Institute of Biomaterials and Bioengineering, Tokyo Medical and Dental University, Tokyo 101-0062, Japan
e-mail: equo.met@tmd.ac.jp

Y. Tanaka · H. Imai
Department of Materials Science and Engineering, Shibaura Institute of Technology, Tokyo 108-8548, Japan

S. Hiromoto
Biomaterials Center, National Institute for Materials Science, Tsukuba 305-0044, Japan

K. Asami
Institute for Materials Research, Tohoku University, Sendai 980-8577, Japan

1 Introduction

Titanium is known to have satisfactory biocompatibility among metallic materials. Several kinds of biomedical alloys were designed till today [1–5]. To develop bone conductivity on titanium, a biomimetic ceramic coating is necessary. The mechanical properties are the result of the characteristics of the bulk structures and that biocompatibility, including bone conductivity, is the result of the surface chemical and/or physical characteristics. Applying a ceramic coating on metals is a promising method to obtain both benefits in one process. Thus, several bioceramic coating techniques, such as bioglass, AW-glass ceramics, and hydroxyapatite ($Ca_{10}(PO_4)_6(OH)_2$), have been developed [6–8].

Plasma spray coating is a well-established ceramic coating technique, and artificial hip joints made of a Ti–6Al–4V alloy coated with hydroxyapatite have been on the market for more than a decade with successful results [9]. The plasma spray coating, however, cannot be applied in sufficient amounts on complex surfaces, such as screws and porous materials. Remaining concerns are the apatite transformation that occurs during remelting at high temperatures and the flaking off of the coated layer [10]. Some other techniques to modify the surface characteristics have been reported.

Ion plating [11] and Ca ion implantation [12, 13] are effective methods, but they require the use of large facilities.

On the other hand, electrochemical treatments are commonly used to form an apatite coating on a titanium substrate. Ban and his colleagues reported on the morphology control of an apatite coating on a titanium substrate using electrolysis techniques at higher temperatures with varied currents [14, 15]. Zhu et al. succeeded in producing a Ca- and P-enriched titanium oxide film on a titanium substrate electrochemically with 70 A m^{-2} and 350 V [16]. These processes were also useful to coat a substrate with a complex surface design. Kuroda et al. used a solution containing calcium phosphate ions and hydrogen peroxide at 150 °C to coat hydroxyl apatite with different surface morphologies on a titanium substrate [17]. You et al. recently reported making a hydroxyapatite coating on dental implants with an electrophoretic technique with 20 V [18]. By these electrochemical treatments, carbonate-containing apatite with desirable morphologies, such as a plane, needles, and particles, could be precipitated on titanium. However, the processes reported above require large current, voltage, and/or higher temperatures. By applying a very large current in excess of the passive current density, the passive film on the alloys may be damaged, and active general corrosion might occur. Porous materials and thin textures will be required for future medical technologies, such as microsurgery and tissue engineering. Treatments providing biocompatibility to those materials with complex surfaces and structures will be required. A thin texture woven with thin titanium fibres is considered to be preferable as a scaffold in tissue engineering. When large current and voltage are applied, the already thin texture easily becomes thinner or dissolves by general corrosion. To avoid these outcomes, an electrolytic treatment with lower voltage is among the better solutions.

In the present study, to enhance the calcium phosphate precipitation, electrolytic treatments applying a step potential (SP) or a cyclic potential (CP) at low voltage were carried out using an artificial biofluid to modify the surface characteristics. According to previous reports, several artificial biofluids have been used for electrochemical treatments [19]. Hanks' solution was employed in this study.

An advantageous feature of this method is not to aim to maintain calcium phosphate layer with appropriate thickness on the alloy during the treatment. It is always possible that coated layers formed before implantation will flake off in clinical usage. At a lower voltage, however, this treatment provides small nuclei of precipitation distributed on the alloy surface that act as sites of natural calcium phosphate precipitation in a living body; in other words, the specks serve as sites for new bone growth. This means that the bonding of implants and bone is guaranteed by the nature of the interface between the implant surface and self-grown bone rather than by that between the implant surface and calcium phosphate coating layer formed as a result of the electrolytic treatments.

The immersion test in Hanks' solution was carried out to simulate bone formation in a living body. To evaluate calcium phosphate formation, X-ray photoelectron spectroscopy (XPS) and scanning electron microscopy (SEM) were conducted. XPS is known as a useful method to evaluate very small amounts of precipitation that are often lower than the detection limitations of SEM and energy-dispersive X-ray spectrometry (EDS). Finally, to develop a biocompatible titanium texture as a model scaffold of tissue engineering, electrolytic treatments were applied on a flatly woven titanium texture. Calcium phosphate formation on the titanium texture was also observed using SEM.

2 Experimental

2.1 Specimens and electrolytic treatments

Commercially pure titanium disks with 8 mm and 14 mm in diameter and 2.2 mm in thickness (purity 99.5 mass%) were used in the present study. Specimens were mechanically polished with SiC papers in de-ionised water and mirror-finished with diamond paste. After being washed ultrasonically in acetone, they were dried with a nitrogen gas flow.

Two kinds of electrolytic treatments using SP and CP with low voltage were developed in the present study. Hanks' solution (pH 7.4), which simulates the inorganic composition of extracellular fluid, was employed as an electrolyte for surface modification. Schematics of the treatment procedures (applied voltage) are shown in Fig. 1.

As shown in Fig. 1(a), SP was applied in one treatment. It was a typical chronoamperometry that measured the current density change while the potential increased step-like from the rest potential, E_0, to 1.0 or 2.0 V, which was a lower voltage than that in conventional methods and still in the passive state. This treatment was performed in two different durations, 1 ks and 10 ks. A potentiostat (HZ-3000, Hokuto Denko) was used to control the potential for the SP treatment. A saturated calomel electrode (SCE) was used as a reference electrode, and platinum was used as

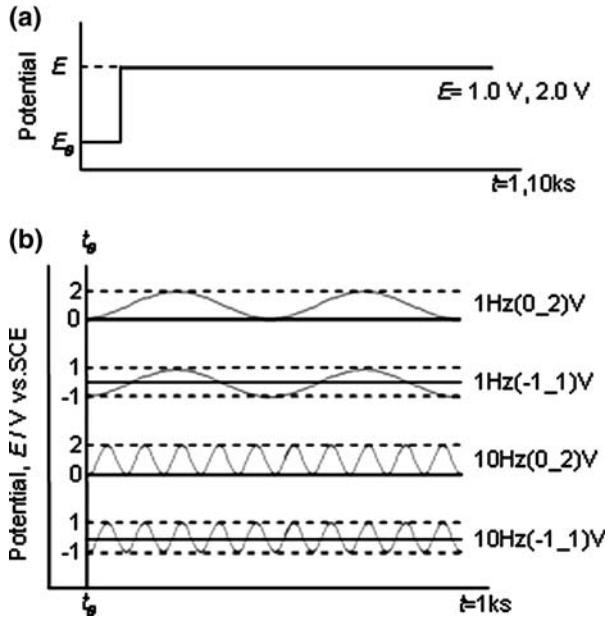

Fig. 1 Schematics of the treatment procedures showing the potential wave forms of the SP treatment (**a**) and the CP treatment (**b**)

a counter electrode. A titanium disk specimen in a Teflon holder, which was insulated from the electrolyte except for an opening window for testing, was used as a working electrode. A schematic of the working electrode is shown in Fig. 2.

In another treatment, CP with a trigonometric wave form was applied with 1 Hz or 10 Hz in frequency instead of SP, as shown in Fig. 1(b). Two different voltage waves with the same amplitude from 0 V to 2.0 V and from –1.0 V to 1.0 V were applied. For this

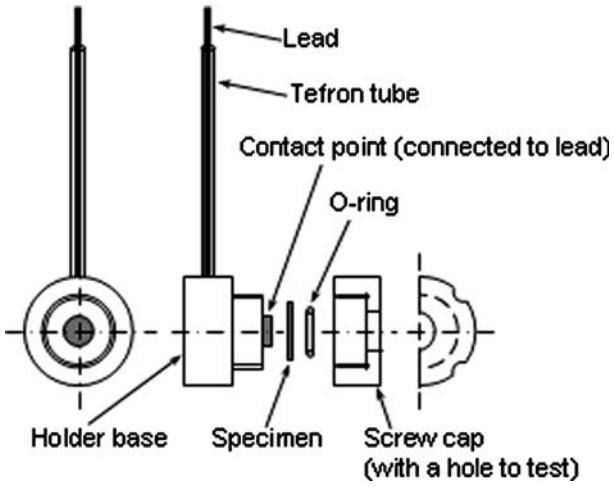

Fig. 2 Schematics of the working electrode including the specimen (titanium disk) and Teflon holder used for the SP and CP treatments. The screw cap has an opening for the test

CP treatment, a function generator (WF1946A, NF Corporation), a data acquisition system (Daq Book, Toyo Corporation), a potentiostat (HZ150G, Hokuto Denko), and data acquisition software (DASY Lab32, ADTEK System Science) to maintain the cyclic wave form were used instead of HZ–3000 in the SP treatment.

For both treatments, a test cell filled up with Hanks' solution was put in an isothermal water bath to keep the electrolyte at 310 K. The electrolyte was deaerated by high-purity nitrogen gas bubbling for 1.8 ks prior to the test.

2.2 Performance of calcium phosphate formation by immersion in Hanks' solution

To evaluate calcium phosphate formation on the surface-modified specimens, immersion in Hanks' solution was carried out after the electrolytic treatments. The specimens were immersed in Hanks' solution (42 ml) at 310 K for 1.0 Ms using sealed Teflon vessels.

2.3 XPS analysis

XPS was carried out using an X-ray photoelectron spectrometer (SSX100, SSI) in order to characterise the specimens' surface of specimens, that of after the electrolytic treatment, and that of after the electrolytic treatment and immersion in Hanks' solution. The X-ray source was monochromatised AlK_α (1486.61 eV) accelerated with 10 kV. The photoelectrons were detected through 20 eV in FAT pass energy, with a 35° take off angle.

The binding energy on the XPS spectra was corrected according to a peak binding energy of C 1s (hydrocarbon C–C and C–H) electrons at 285.0 eV due to the surface-contaminated layer [20]. The quantification of the composition and the thickness measurement of the surface films and layers were conducted with the inductive calculation method presented by Asami et al. [21], assuming stacking layers of a titanium oxide film (inner layer), a calcium phosphate layer (intermediate layer), and carbon contaminants (outer layer) on a titanium substrate.

2.4 SEM/EDS analysis

To evaluate the characteristics of calcium phosphate after immersion in Hanks' solution, SEM/EDS analysis was conducted with secondary electron images of a scanning electron microscope (JSM-5400, JEOL) at 15 kV of accelerating voltages and energy-dispersive

X-ray spectrometry (EDS) at 10 kV of accelerating voltage with 0.8 A of current density.

2.5 Electrolytic treatments on the titanium texture

In order to develop a biocompatible titanium texture, CP treatments were applied on a flatly woven titanium texture (1.0 mm in texture width, woven with eight titanium wires with a wire diameter of 0.1 mm) provided by Dr. K. Murakami of Ishikawajima-Harima Heavy Industries. Calcium phosphate formation through immersion in Hanks' solution on the titanium woven texture was observed using SEM.

3 Results

3.1 SP treatment

3.1.1 Current density response curves

The current density response curves of the SP treatments at 1.0 V for 1 ks and 10 ks are shown in Fig. 3. An inserted graph shows a close-up view of the curves within tens of seconds after the SP. The curve of the 1 ks treatment precisely overlapped with that of the 10 ks treatment even in this enlarged figure. The SP treatments at 2.0 V also showed almost identical curves. When the potential was changed from the rest potential, E_0, to a step potential (1.0 V or 2.0 V), the peak current density, I_0, appeared as the maximum value followed by steep decreasing to a very small passive current density with an asymptotic curvature. The total electric charge, Q, was calculated as a time-transient curve of the current density. For both treatment times (1 ks and 10 ks), no difference between Q and I_0 was seen because the current density had decreased asymptotically and was close to zero (in fact, it reached zero within the current resolution of the measurement system in the present study) before 1 ks. The values of I_0 and Q for each test condition are indicated in Table 1.

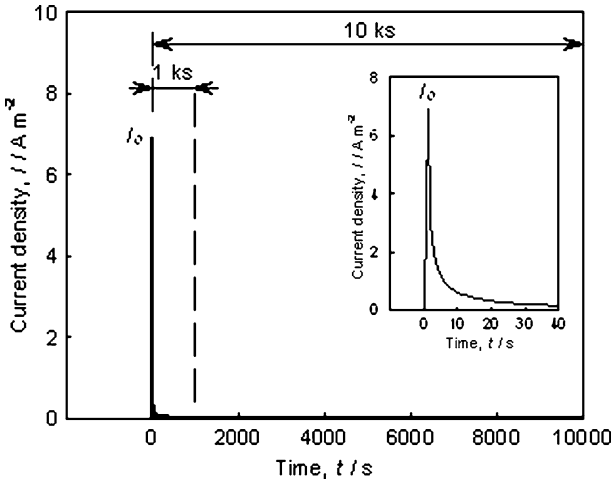

Fig. 3 Current density response curves of the SP treatments at 1.0 V for 1 ks and 10 ks showing the peak current density, I_0, and the steep decrease of the current density. An inserted graph shows a close-up view of the curves within tens of seconds after the SP

After these treatments, no sign of corrosion, including pitting and general corrosion, was observed.

3.1.2 XPS analysis

The surfaces of SP-treated specimens exhibited a slightly golden lustre. The specimen treated at 2.0 V for 10 ks had the darkest shade of golden lustre among them. This suggested the presence of some reaction product on the film that contained yellowish ions and/or interfered with the colouring on the specimens' surface. The results of a wide range of XPS spectra are shown in Fig. 4. In the spectrum of each specimen, peaks from C, O, Ti, P, Ca, and/or N were detected.

The compositions of surface films of specimens with/without SP treatment are shown in Table 2. No Ti was detected form the specimen treated at 2 V for 10 ks, while P and Ca were detected in each specimen. This suggests that a very thick phosphate layer was formed on the titanium oxide film on the surface of the specimen treated at 2.0 V for 10 ks.

Figure 5 shows the XPS analysis of the Ti 2p electron energy region on the surfaces of all specimens. The XPS spectra were decomposed into four doublets (Ti^0, Ti^{2+}, Ti^{3+}, and Ti^{4+}) with the valence according to the binding energy reported by Asami et al. [22]. All of the specimens, other than those treated at 2.0 V for 10 ks, showed Ti $2p_{3/2}$ (higher binding energy) and Ti $2p_{1/2}$ (lower) peaks of Ti^{4+}. In addition, only the untreated specimen showed a clear spectrum peak of Ti^0, which corresponds to the metallic state. A fraction of Ti^{4+} among all Ti cations, Ti^{2+}, Ti^{3+}, and Ti^{4+}, is shown in Table 3 together with the surface film

Table 1 Results of the SP treatment for the peak current density, I_0, and the total electric charge, Q, which was calculated as a time-transient curve of the current density

	Step potential	
	1 V	2 V
I_0 (A m^{-2})	6.5	6.5
Q (C m^{-2})	3.5×10^{1}	3.7×10^{1}

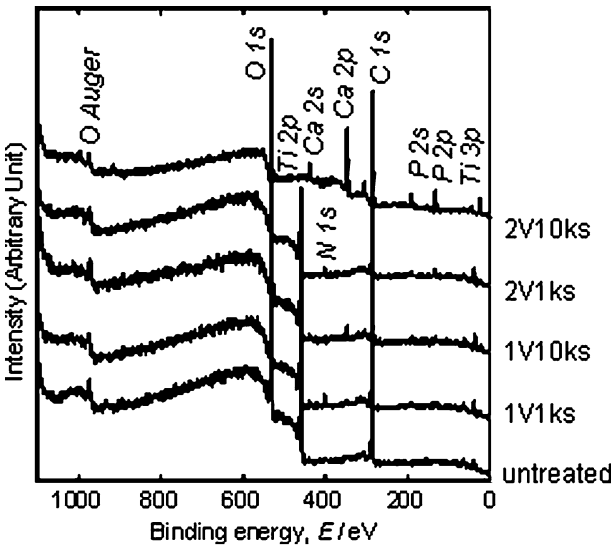

Fig. 4 Results of wide-range XPS spectra of SP-treated specimens in comparison with an untreated specimen showing C, O, Ti, P, Ca, and/or N peaks

Table 2 Compositions of the surface films of the specimens after SP treatment calculated from XPS data

	Ti	O	P	Ca
1 V–1 ks	17.19	80.79	1.63	0.38
1 V–10 ks	58.09	23.33	9.41	9.17
2 V–1 ks	18.47	79.15	2.14	0.24
2 V–10 ks	0	83.23	6.10	10.67
				(mol %)

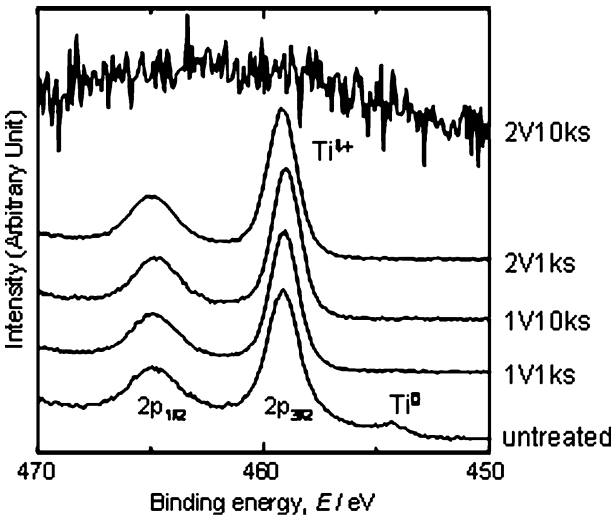

Fig. 5 Ti 2p electron energy region XPS spectra of SP-treated specimens showing Ti $2p_{3/2}$ and Ti $2p_{1/2}$ peaks of Ti^{4+}. Only the untreated specimen's spectrum showed a Ti^0 peak

thickness calculated from the XPS data. As compared to the specimen without treatment, all of the SP-treated specimens exhibited around 67% thicker surface films and an approximately 12% higher Ti^{4+} fraction. However, no significant difference in the thickness and the Ti^{4+} fraction was seen among specimens treated at 1.0 V for 1 ks, 1.0 V for 10 ks, and 2.0 V for 1 ks. The results for the specimen treated at 2.0 V for 10 ks in Tables 2 and 3 reveal that a very thick phosphate layer was formed above the titanium oxide film, which prevented the detection of any titanium cation peaks, as shown in Fig. 5.

Spectra of P 2p and Ca 2p were obtained as a set of peaks. The binding energy of P 2p electrons was 133.3–133.5 eV, while that of Ca 2p3/2 electrons was 347.3–347.6 eV in a previous study [23, 24]. According to these data, the former spectrum overlapped in the vicinity of two peaks coming from PO_4^{3-} and HPO_4^{2-}, and the latter, in the vicinity of those coming from Ca^{2+}, proving the calcium phosphate formation. The spectra of O 1s were also decomposed into three peaks of O^{2-} (oxides), OH^- (hydroxides or hydroxyl group), and H_2O (bound water or adsorbed water) [25]. The ratio of Ca and P ([Ca]/[P]) and the fraction of the OH^- in all oxygen atoms, $[OH^-]/([O^{2-}] + [OH^-] + [H_2O])$, are shown in Fig. 6. The [Ca]/[P] ratio increased in the order of 2.0 V for 10 ks: 1.0 V for 10 ks: 1.0 V for 1 ks : 2.0 V for 1 ks. These two data showed strong correspondence. The largest ratio in the specimen treated at 2.0 V for 10 ks was 1.75, which was almost identical to that of the hydroxyapatite nominal, 1.67. The same specimen showed the largest OH^- fraction, which was 0.75.

This calcium phosphate formation was reconfirmed by the SEM/EDS analysis. Figure 7 indicates the result of EDS analysis of the specimen treated at 1.0 V for 1 ks after immersion in Hanks' solution. The peaks from Ca and P, which are precipitated during immersion in Hanks' solution, are identified.

3.2 CP treatment

3.2.1 Current density response curves

The current density response curve during CP treatment at 1 Hz with –1.0 to 1.0 V is shown in Fig. 8. The maximum anodic current in each cycle of a potential wave decreased asymptotically when the testing time elapsed, while the minimum cathodic current exhibited a small fixed current around –5.0 A m^{-2}. In the case of the treatment at the same frequency with 0–2.0 V, a curve with the same tendency but drawn only in the anodic side (the minimum current was just on the

Table 3 Thickness and fraction of Ti^{4+} among all Ti cations (Ti^{2+}, $Ti3^{+}$, and Ti^{4+}) in the oxide film formed on the specimens with/without SP treatment

	Treatment conditions			
	Untreated	1 V–1 ks	1 V–10 ks	2 V–1 ks
Thickness of surface oxide (nm)	3.6	5.9	6.1	6.0
$[Ti^{4+}]/([Ti^{2+}] + [Ti^{3+}] + [Ti^{4+}])$	0.82	0.91	0.91	0.94

The thickness was calculated from XPS data according to Asami's inductive method [21]

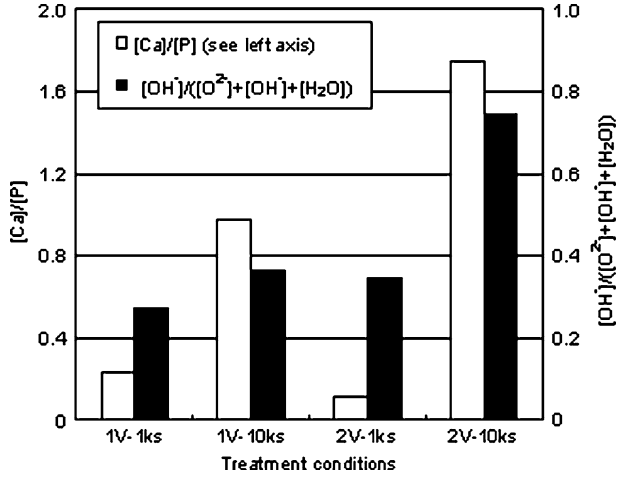

Fig. 6 Ratio of [Ca]/[P] and the fraction of the OH^- in all oxygen atoms $[OH^-]/([O^{2-}] + [OH^-] + [H_2O])$ of the surface oxide films on SP-treated specimens

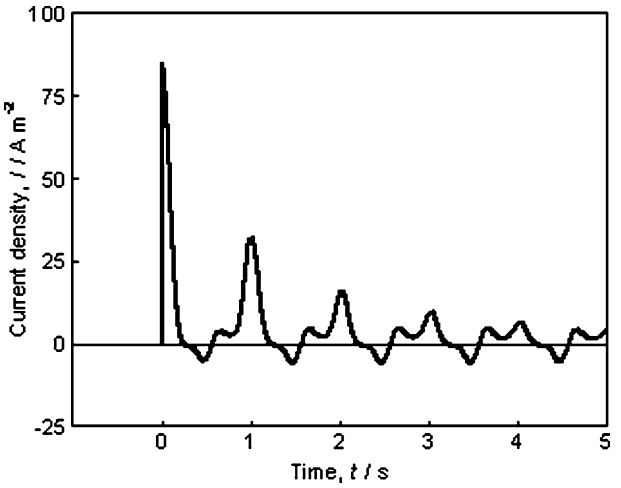

Fig. 8 Current density response curve during 1 Hz (–1_1)V CP treatment. The potential waves from were –1.0 V to 1.0 V at 1 Hz in frequency

abscissa) was obtained. For the CP treatments at 10 Hz with –1.0 to 1.0 V and 0–2.0 V, similar wave forms to 1 Hz with ten times faster frequency were seen.

No mark of pitting and general corrosion was observed in each specimen after these treatments.

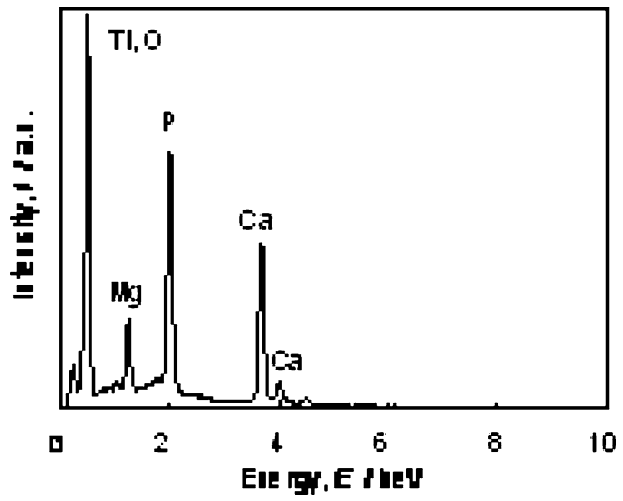

Fig. 7 SEM/EDS analysis of specimens treated at 1.0 V for 1 ks after immersion in Hanks' solution indicating peaks from Ca and P

3.2.2 *XPS analysis*

After the CP treatment, the surfaces of the specimens achieved a pale golden lustre, suggesting that the reaction products formed in the same way as with the SP treatment. The lustre was paler than that of SP-treated specimens at 2.0 V for 10 ks. Wide-range XPS analysis detected peaks from C, O, Ti, P, Ca, and/or N in each spectrum as well.

The compositions of the surface films are indicated in Table 4. In each specimen, O occupied around 80 mol % of the surface films, which was O^{2-}, OH^-, and H_2O. Specimens after CP treatment with 0–2.0 V exhibited higher Ti contents than those after CP treatment with –1.0 to 1.0 V.

The surface film thickness calculated from the XPS data and the fraction of Ti^{4+} in the oxide film are indicated in Table 5. Showing a certain correspondence between the thickness and Ti^{4+} fraction, the minimum of both data was seen in the specimen treated at 1 Hz with 0–2.0 V (4.9 nm in thickness and 0.88 in fraction), and the maximum, in the specimen at 10 Hz with 0–2.0 V (5.6 nm in thickness and 0.93 in fraction).

Table 4 Compositions of the surface films of the specimens after CP treatment calculated from XPS data

	Ti	O	P	Ca
1 Hz (0_2) V	21.19	77.56	1.01	0.13
1 Hz (–1_1) V	13.32	83.94	1.91	0.83
10 Hz (0_2) V	20.60	77.85	1.32	0.23
10 Hz (–1_1) V	18.15	78.84	1.41	1.60
				(mol %)

The spectra of P 2p and Ca 2p were also determined to come from PO_4^{3-}, HPO_4^{2-}, and Ca^{2+}, in the same way as for SP-treated specimens. The [Ca]/[P] ratio and the ratio of $[OH^-]/([O^{2-}] + [OH^-] + [H_2O])$ are shown in Fig. 9. For both the [Ca]/[P] ratio and the fraction of OH^-, the specimens treated with the potential wave from –1.0 V to 1.0 V were larger than those treated only with the anodic current (0–2.0 V). This suggests that the cathodic current might have an effect on calcium phosphate precipitation.

3.3 Calcium phosphate formation

Figure 10 shows secondary electron images of the surface of specimens after immersion in Hanks' solution for 1.0 Ms; these images correspond to SP-treated and untreated specimens. In the EDS analysis carried out simultaneously, P, Ca, and Mg were identified in the precipitates on the surface, which suggested the formation of calcium phosphate-containing magnesium. Ban and Maruno [26] also reported that the magnesium in the calcium phosphate layer was deposited on the titanium after an electrochemical treatment using a simulated body fluid. The amount of calcium and magnesium increased proportionally to the square root of the treatment time and the cathodic potential. Comparing the SEM images, no significant difference on precipitate formation was seen between the untreated specimen and specimens treated for 1 ks. The number of calcium phosphate particles, however, obviously increased with increasing the treatment time up to 10 ks.

The results of immersion for CP-treated specimens are shown in Fig. 11. Cracks were observed in the base calcium phosphate layer formed during the CP treatment. In comparison with calcium phosphate formation during immersion, the specimens treated at –1.0 to 1.0 V showed a larger amount of precipitate.

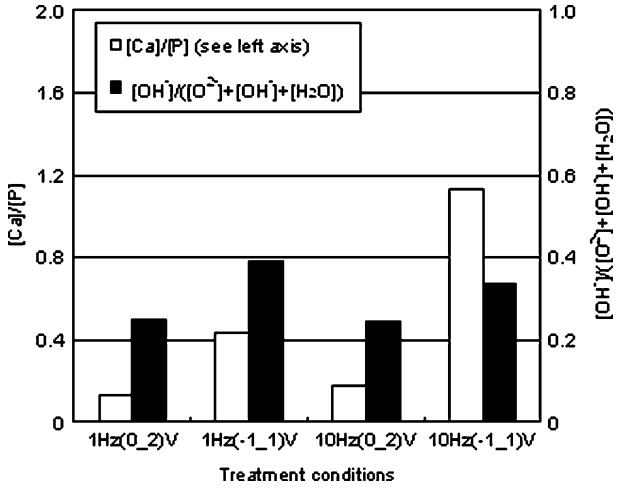

Fig. 9 Ratio of [Ca]/[P] and the fraction of the OH^- in all oxygen atoms $[OH^-]/([O^{2-}] + [OH^-] + [H_2O])$ of the surface oxide films on CP-treated specimens

3.4 Electrolytic treatments for titanium texture

SEM micrographs of a titanium woven texture after CP treatments at 1 Hz with –1.0 to 1.0 V followed by Hanks' solution immersion for 1.0 Ms are shown in Fig. 12. In the higher magnification on the right, calcium phosphate precipitates of around 5 μm in particle size were clearly identified with EDS. No corrosion was observed, even at higher magnification.

4 Discussion

4.1 Effects of electrolytic treatments on the surface films

The phenomenon that occurred in the electrolytic cell while the potential increased from the rest potential, E_0, to 1.0 or 2.0 V of the step potential in the SP treatment can be considered to be a charge/discharge process of the total electric charge, Q, to/from a condenser (an electric double layer) through a resistant

Table 5 Thickness and fraction of Ti^{4+} among all Ti cations in oxide film formed on the specimens after CP treatment.

	Treatment conditions			
	1 Hz(0_2) V	1 Hz (–1_1) V	10 Hz (0_2) V	1 Hz 0 (1_1) V
Thickness of surface oxide (nm)	4.9	5.3	5.6	5.1
$[Ti^{4+}]/([Ti^{2+}] + [Ti^{3+}] + [Ti^{4+}])$	0.88	0.90	0.93	0.91

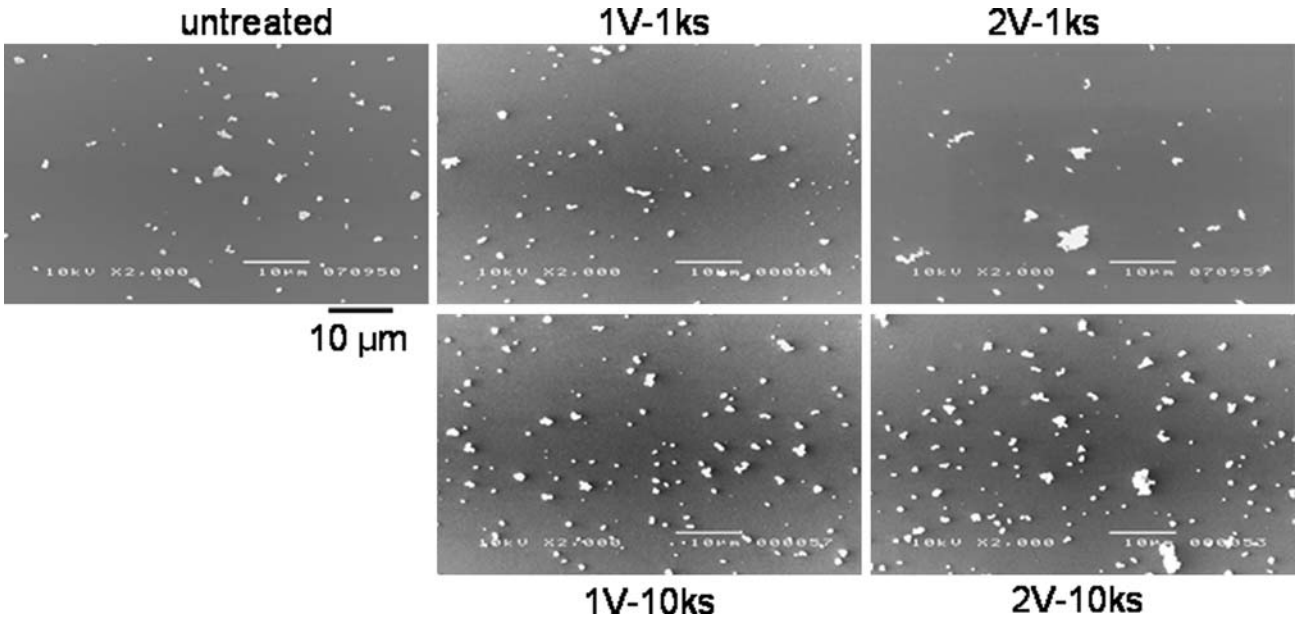

Fig. 10 SEM secondary electron images of the surface of the specimens of SP-treated and untreated specimens after immersion in Hanks' solution for 1.0 Ms, showing calcium phosphate precipitates

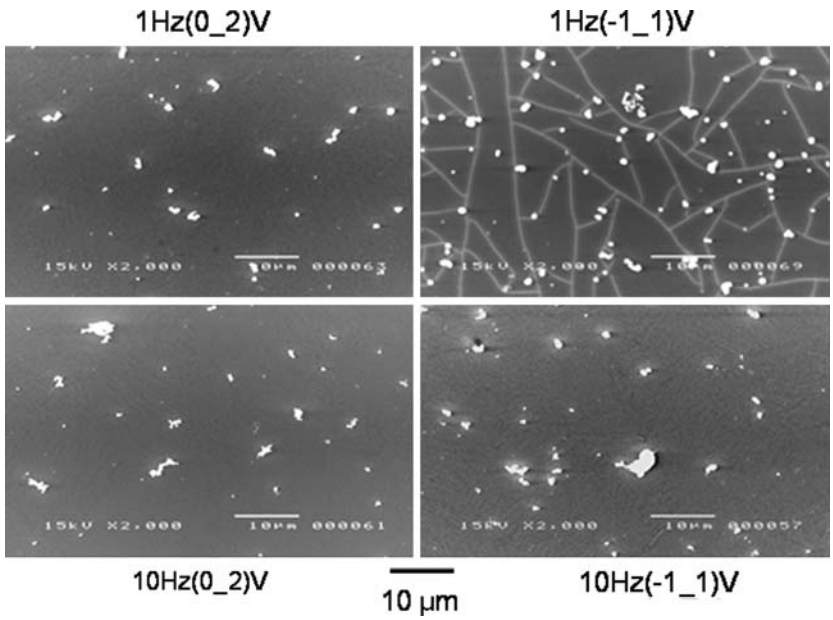

Fig. 11 SEM secondary electron images of the surfaces of specimens after CP treatment followed by immersion in Hanks' solution for 1.0 Ms. Cracks were observed in the base calcium phosphate layer on the 1 Hz(–1_1)V specimen

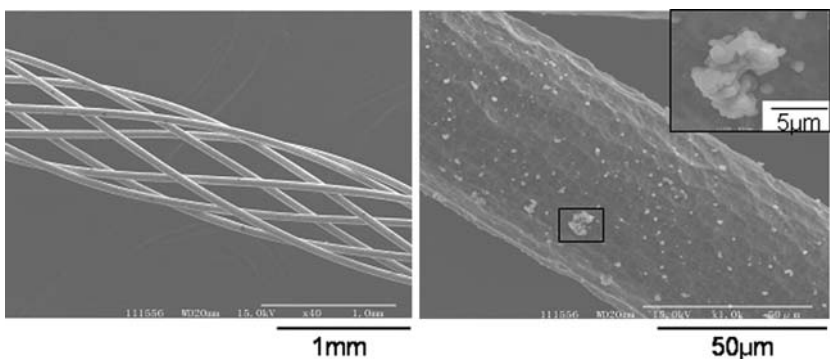

Fig. 12 SEM micrographs of a titanium woven texture after CP treatments, 1 Hz (–1_1)V, followed by immersion in Hanks' solution for 1.0 Ms. Calcium phosphate precipitates are seen in a close-up view on the right

material (Hanks' solution). The total electric charge, Q, can be calculated from the time-transient curve of the current density, and the current is controlled by the electron (ion) transfer in the testing system. When the potential is increased from the rest potential, E_0, to 1.0 V or 2.0 V, the electrons transfer from the electrolyte to the electrode. If the potential gap between the specimen and the electrolyte is larger, the electron migration becomes easier and faster just after the SP change. Then, with higher SP, the anodic current became larger. In fact, a larger total electric charge, Q, was observed at 2.0 V SP. After the electron transfer, the potential gap (including a gradient within the electric double layer) settled again in an equilibrium passive condition.

After the SP and CP treatments, the surface of titanium had a golden lustre due to the reaction product on the film that contained yellowish ions and/or showed interference colouring. The SP treatment at 2.0 V for 10 ks, which had the darkest golden lustre in the present study, was expected to have the thickest surface film formation of any treatment conditions. This thick film (layer) contained not only titanium oxide but also a certain amount of calcium phosphate [24, 27]. This means that calcium phosphate precipitation occurred during the SP treatment (before immersion in Hanks' solution) as a result of the longer treatment time.

4.2 Titanium stability in surface films

In the XPS analysis of the surfaces of the specimens after SP treatment, C, O, Ti, Ca, P, and/or N spectra were detected from the oxide films. Among them, C and N were considered to exist as a contaminated layer, and O, as oxides. Except for the SP treatment at 2.0 V for 10 ks, which exhibited no clear Ti^{4+} peaks due to the thick calcium phosphate layer, no significant difference was observed in the fraction of Ti^{4+}. Because TiO_2 is the most stable form in the titanium oxides, this Ti^{4+} fraction is considered as the stability of oxide. From these data, the SP treatment produced a thicker and more stable oxide film than that of the untreated specimen.

The thickness of the oxide film on the CP treated specimens was approximately 5 nm regardless the treatment conditions showing small difference and fraction of Ti^{4+} was varied from 88% to 93% and showed a similar tendency in thickness.

Although neither the frequency nor the different treatments, –1.0 V to 1.0 V and 0 V to 2.0 V, revealed clear effects, there was a certain correspondence between the oxide film thickness and oxide stability.

4.3 Calcium phosphate precipitation during electrolytic treatments

The fraction of OH^- among O^{2-}, OH^-, and H_2O in SP-treated specimens, as shown in Fig. 6, became larger with the treatment time. The specimens treated with 2.0 V for 10 ks showed the largest fraction of OH^-, which was larger than that of untreated specimen. The largest [Ca]/[P] ratio (1.75) was seen in the same specimen among all test conditions. For both step potentials, the very small passive current density longer than 10 ks is still effective to increase the [Ca]/[P] ratio and the OH^- fraction. Thus, the hydroxyl group might have a certain effect on the crystallinity of the calcium phosphate.

In the CP treatment at 1 Hz and 10 Hz with –1.0 V to 1.0 V, as shown in Fig. 9, the cathodic current might be a factor to form the high [Ca]/[P] ratio calcium phosphate. Moreover strong correspondence was seen between the [Ca]/[P] ratio and the hydroxyl group fraction, which suggested the hydroxyl group affected the crystallinity of the calcium phosphate in the same manner as the SP treatment. It is suggested that the cyclic exchange of anodic and cathodic currents may enhance the absorption of P and Ca alternately and that OH^- may contribute to this process.

4.4 Immersion in Hanks' solution to precipitate the calcium phosphate layer

The calcium phosphate formation of specimens SP-treated for 10 ks after immersion in Hanks' solution was comparable to that of the untreated specimen. The XPS data (no Ti^0 peak identified in specimens treated at 1.0 V for 1 ks, 1.0 V for 10 ks, 2.0 V for 1 ks and 2.0 V for 10 ks specimens) and the SEM observation suggest that the calcium phosphate precipitated not only as particles, but as a thin layer covering the surface of each specimen. The number of calcium phosphate precipitates increased with the increasing treatment time. Even though the passive current density from 1 ks to 10 ks was very small, it was still an important factor for particle precipitation and growth of the layer of the calcium phosphate. The effect of the SP difference on the precipitation was not identified within the conditions of the present study.

The immersion in Hanks' solution after CP treatment also produced both layer and particle calcium phosphate. Differently from the case of the SP treatment, cracks in the base phosphate layer on the surface treated at –1.0 V to 1.0 V were observed. These cracks were clearly caused by the thickness of the layer. However, a more detailed discussion of these cracks

and the cathodic current would exceed the scope of the present study. The number of precipitates obviously increased in the treatment at –1.0 to 1.0 V.

As stated above, both the very small passive current (in the SP treatment) and the cathodic current (in the CP treatment with –1.0 to 1.0 V) were effective to accelerate the calcium phosphate formation. Although the mechanisms in either case may differ, they have not been clearly identified. As shown in Figs. 6 and 9, the existence of the hydroxyl group shows a certain correlation to calcium phosphate formation. It is strongly suggested that the hydroxyl group affects the absorption of Ca and P ions and/or the formation of calcium phosphate on the surface. The very small passive current in the SP treatment and the cathodic current in the CP treatment might have a role in this process.

5 Conclusion

Calcium phosphate was precipitated on a titanium surface by the SP and CP treatments together with a titanium oxide film. In the SP treatment, the stability of the oxide thickness of the oxide film and the fraction of the hydroxyl group on the surface became larger with a longer treatment time. In the CP treatment, the stability of the oxide thickness of the oxide film and the fraction of the hydroxyl group on the surface became larger in the treatment with a potential wave at –1.0 to 1.0 V rather than at 0–2.0 V. The very small passive current in the SP treatment and the cathodic current in the CP treatment enhanced the calcium phosphate formation. SP and CP treatments were effective to accelerate calcium phosphate precipitation on titanium in Hank's solution in spite of their lower voltage than that of the conventional methods. The calcium phosphate formation was accelerated by the hydroxyl group in Hanks' solution.

References

1. A. K. SHUKLA, R. BALASUBRAMANIAM and S. BHARGAVA, J. Alloys Compd. **389** (2005) 144
2. E. EISENBARTH, D. VELTEN, M. MULLER, R. THULL and J. BREME, Biomaterials **25** (2004) 5705
3. J. I. QAZI, B. MARQUARDT and H. J. RACK, JOM **56** (2004) 49
4. M. TAKAHASHI, E. KOBAYASHI, H. DOI, T. YONEYAMA and H. HAMANAKA, J. Jpn Inst. Metals **64** (2000) 1120
5. E. KOBAYASHI, H. DOI, T. YONEYAMA, H. HAMANAKA, I. R. GIBSON, S. M. BEST, J. C. SHELTON and W. BONFIELD, J. Mater. Sci. Mater. Med. **9** (1998) 625
6. T. KITSUGI, T. NAKAMURA, M. OKA, Y. SENAHA, T. GOTO and T. SHIBUYA, J. Biomed. Mater. Res. **30** (1996) 261
7. V. A. DUBOK, *Powder Metall. Met. Ceram.* **39** (2000) 381
8. L. M. SUN, C. C. BERNDT, K. A. GROSS and A. KUCUK, J. Biomed. Mater. Res. **58** (2001) 570
9. W. J. A. DHERT, Med. Prog. Technol. **20** (1994) 143
10. M. FINI, A. CIGADA, G. RONDELLI, R. CHIESA, R. GIARDINO, G. GIAVARESI, N. N. ALDINI, P. TORRICELLI and B. VICENTINI, Biomaterials **20** (1999) 1587
11. M. YOSHINARI, Y. OHTSUKA and T. DERAND, Biomaterials **15** (1994) 529
12. T. HANAWA, Y. NODASAKA, H. UKAI, K. MURAKAMI and K. ASAOKA, J. Jpn Soc. Biomater. **12** (1994) 209
13. T. HANAWA, Y. KAMIURA, S. YAMAMOTO, T. KOHGO, A. AMEMIYA, H. UKAI, K. MURAKAMI and K. ASAOKA, J. Biomed. Mater. Res. **36** (1997) 131
14. S. BAN and S. MARUNO, Biomaterials **19** (1998) 1245
15. S. BAN and J. HASEGAWA, Biomaterials **23** (2002) 2965
16. X. L. ZHU, K. H. KIM and Y. S. JEONG, Biomaterials **22** (2001) 2199
17. K. KURODA, Y. MIYASHITA, R. ICHINO and M. OKIDO, Mater. Sci. Forum **426–4** (2003) 3189
18. C. K. YOU, X. W. MENG, T. Y. KWON, Y. Z. YANG, J. L. ONG, S. KIM and K. H. KIM, Bioceramics **17** (2005) 901
19. T. HANAWA, K. ASAMI and K. ASAOKA, J. Biomed. Mater. Res. **40** (1998) 530
20. K. ASAMI, J. Electr. Spectrosc. **9** (1976) 469
21. K. ASAMI, K. HASHIMOTO and S. SHIMODAIRA, Corros. Sci. **17** (1977) 713
22. K. ASAMI, S. C. CHEN, H. HABAZAKI and K. HASHIMOTO, Corros. Sci. **35** (1993) 43
23. T. HANAWA and M. OTA, Biomaterials **12** (1991) 767
24. T. HANAWA and M. OTA, Appl. Surf. Sci. **55** (1992) 269
25. K. ASAMI and K. HASHIMOTO, Corros. Sci. **17** (1977) 559
26. S. BAN and S. MARUNO, Jpn J. Appl. Phys. **32** (1993) L1577
27. K. E. HEALY and P. DUCHEYNE, J. Biomed. Mater. Res. **26** (1992) 319